

Spin of Single Electron Traps in Silicon Nanowire-based Transistors

M. Hofheinz,* X. Jehl, and M. Sanquer
CEA-DRFMC, 17 rue des Martyrs, F-38054 Grenoble cedex 9, France

G. Molas, M. Vinet, and S. Deleonibus
CEA-LETI, 17 rue des Martyrs F-38054 Grenoble cedex 9, France
(Dated: December 2, 2024)

We report experiments using nanowire-based silicon single electron transistors to monitor the occupation of individual charge traps located in the nanowire. Comparison with a computer simulation of the Coulomb blockade spectrum in presence of a charge trap allows us to determine the nature, position and spin of the traps. They are attributed to As donor states.

PACS numbers: 73.23.Hk, 71.70.Ej, 72.20.My

Keywords: Coulomb blockade; coupled quantum dots; Zeeman effect; silicon nanowires

I. INTRODUCTION

Recently it has become possible to detect individual electron spins in quantum dots — optically¹ or electrically²⁻⁴. In the electrical measurements the Zeeman effect shifts the electron level above or below the Fermi energy, depending on the spin polarization. This way the spin polarization is related to the occupation number of the electronic state. Such measurements therefore rely on the detection of a single electron charge. Quantum point contacts in GaAs heterostructures⁴ and random telegraph noise in a silicon field effect transistor^{2,3} have been used for this purpose, as well as metallic single electron transistors (SETs)⁵.

We use nanowire-based silicon transistors operated as SET at low temperature to detect the occupation number of individual charge traps. They are capacitively coupled to the SET. Therefore they induce anomalies in the otherwise very regular periodic oscillations of the drain-source conductance G versus gate voltage V_g . We compare the data with simulations obtained after solving the master equation for the electrostatic network formed by the main dot and the charge trap. A magnetic field was applied in order to probe the spin polarization of the traps via their Zeeman shifts. As expected from simple considerations⁶, we observed a majority of singly occupied traps. This is in contrast with Refs. 2,3 where only doubly occupied trap states were reported.

The good electrostatic control of our system, its excellent stability in time as well as its full compatibility with CMOS technology make it a promising candidate for spintronics realizations.

II. SAMPLES AND MEASUREMENTS

Samples are produced on 200mm wafers in a large-scale microelectronics facility. A 30 nm wide and 200 nm long nanowire is etched from a 17 nm silicon-on-insulator (SOI) film. A 40 nm long polysilicon control gate is deposited in the middle of the wire (see Figs. 1(a) and 1(b)).

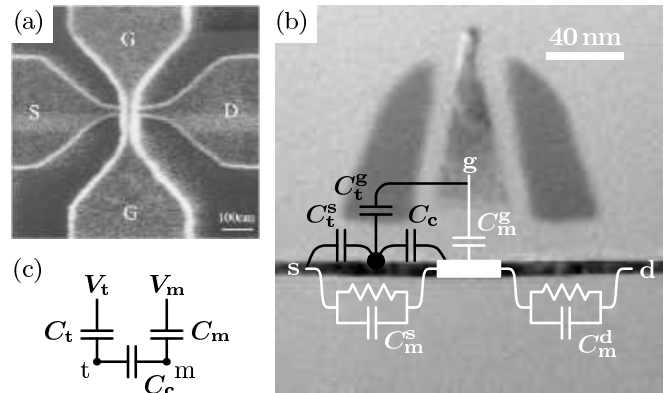


FIG. 1: Sample layout and electrical model: (a) Top view of the sample before back-end process obtained in a scanning electron microscope. (b) Transmission electron micrograph along the silicon nanowire (black). The wire shown here is thinner than in the samples used for measurements. Light gray regions are silica. The darker region in the center is the polysilicon gate stack, surrounded by Si_3N_4 spacers. Superimposed is the equivalent electrical circuit of our model. The main dot (m) is drawn in white, the trap state (t) in black. The positions of the resistors and capacitors of the access regions are shifted for clarity. (c) Simplified electrical circuit for electrostatic considerations.

The gate-covered region of the wire defines the quantum dot. With respect to earlier samples⁷ the gate oxide thickness t_{ox} is now 24 nm (or 10 nm), instead of 4 nm before. It consists of a 4 nm (or 2 nm) thermal oxide and a 20 nm (or 8 nm) deposited oxide. 50 nm-wide Si_3N_4 spacers are now added on both sides of the gate electrode. They allow for a lower doping level (As, 10^{18} cm^{-3}) in the vicinity of the gate. In the uncovered regions of the wire, an optimized ion implantation process ensures good crystalline structure despite the high doping level of $5 \cdot 10^{19} \text{ cm}^{-3}$. This two-step implantation process yields low defect concentration near the active channel of the transistor. Several samples have been measured but for clarity we present results for only two typical examples.

Measurements were taken in a dilution refrigerator

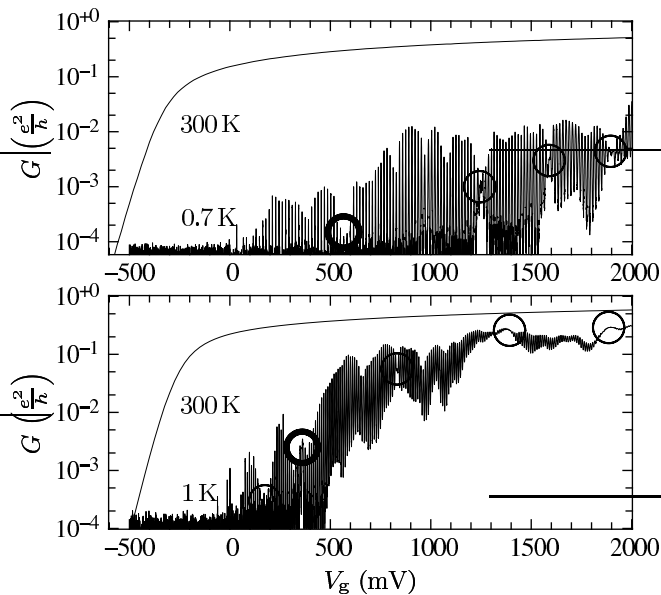


FIG. 2: Drain-source conductance versus gate voltage for the two samples presented in this paper. They have the same geometry, only the gate oxide thickness differs (24 nm in the upper panel and 10 nm in the lower panel). The smooth field-effect characteristic at room temperature is replaced by very periodic Coulomb blockade oscillations at low temperature. The period is determined by the surface area of the nanowire/gate overlap. Anomalous regions with reduced contrast and fluctuating peak spacing are highlighted with circles. The anomalies marked with bold circles are studied in detail in Fig. 3 for the upper panel and Fig. 5 for the lower one.

at 70 mK (except data in Fig. 2). However, the effective electronic temperature, deduced from the width of Coulomb blockade resonances, is approximately 10 times higher (see below). We used a standard 2-wire lock-in technique at 177 Hz and voltage excitation low enough to stay in linear regime ($100 \mu\text{V}_{\text{rms}}$ for low temperature measurements and $5 \text{ mV}_{\text{rms}}$ for room temperature measurements). For spin sensitive measurements a superconducting magnet was used to apply an in-plane magnetic field of up to 16 T.

III. DATA AND MODEL

Figure 2 shows typical $G(V_g)$ plots. At room temperature our samples behave as classical (albeit not optimized) n -channel MOSFETs. Below approximately 20 K they turn into single electron transistors with regularly spaced Coulomb blockade resonances. The period $V_g^C = \frac{e}{C_m^g}$ of these oscillations is determined by the gate capacitance C_m^g , which in turn can be estimated by the gate/wire overlap and the gate oxide thickness. For the sample with 24 nm (10 nm) gate oxide the peak spacing is $15.3 \text{ mV} \pm 0.8 \text{ mV}$ ($10.3 \text{ mV} \pm 0.5 \text{ mV}$) corresponding to a gate capacitance of 10.5 aF (15.5 aF). As the gate oxide thickness approaches the widths of gate and wire,

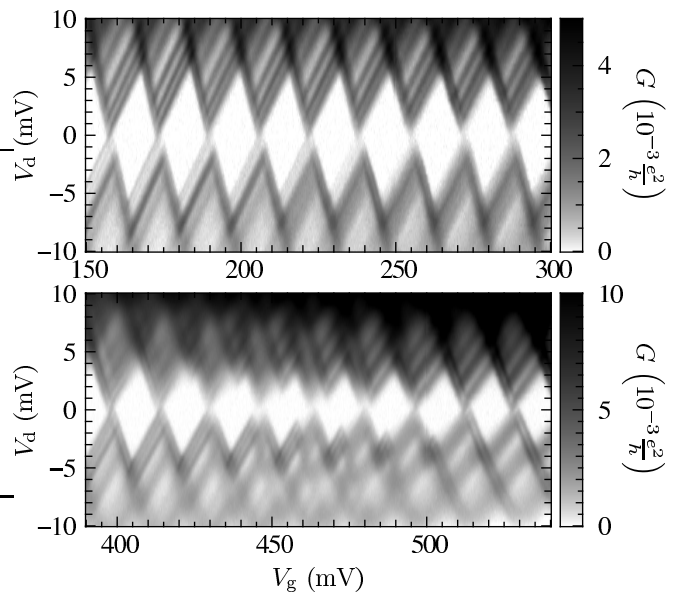


FIG. 3: Stability diagram: 2D-plots of the measured drain-source conductance versus gate and drain voltages in an unperturbed, very periodic gate voltage range (upper panel), and in an anomalous region where a charge trap is observed (lower panel). White areas correspond to Coulomb blocked regions (no detectable current). The lines inside the conducting regions are attributed to localized states in the vicinity of the dot rather than to the single-particle spectrum of the dot (the spacing being too high and almost identical for all resonances). With respect to the measurements in Fig. 2, the anomalous region has shifted slightly in gate voltage after thermal cycling between base and room temperature.

the deviation from the planar capacitor approximation becomes important and the gate capacitance is not exactly proportional to t_{ox}^{-1} . The statistics of the peak spacing in earlier devices (4 nm gate oxide) has already been measured and compared to theory.⁷ Here we report a detailed analysis of anomalous regions where the contrast is markedly reduced and a phase shift of the Coulomb blockade oscillations occurs. This results in tails in the Gaussian peak-spacing distribution. Such perturbations to the periodic pattern are marked with circles in Fig. 2. In the measured stability diagram, i.e. the conductance versus gate and bias voltage plot, the effect is even more striking (see Fig. 3). We developed a simple model based on a trap state located in the vicinity of the quantum dot, and compare the simulation with the experimental data.

The electrical circuit of the model is shown in Fig. 1(b). A small trap (t) is capacitively coupled to source (s), gate (g) and to the main dot (m). For electrostatic considerations the problem can be simplified to the circuit shown in Fig. 1(c), with $C_{m,t} = \sum_{i=s,d,g} C_{m,t}^i$ and $V_{m,t} = \sum_{i=s,d,g} \frac{C_{m,t}^i}{C_{m,t}} V^i$. The electrostatic energy of electrons in the two dots can then be expressed as

$$W(Q_m, Q_t) = \frac{Q_m^2}{2C'_m} + \frac{Q_t^2}{2C'_t} + V'_m Q_m + V'_t Q_t + \frac{Q_m Q_t}{C'_c} \quad (1)$$

with:

$$\begin{aligned} C'_m &= C_m + C_t \parallel C_c && \approx C_m \\ C'_t &= C_t + C_m \parallel C_c && \approx C_t + C_c \\ V'_m &= \frac{C_m V_m + (C_t \parallel C_c) V_t}{C'_m} && \approx V_m \\ V'_t &= \frac{C_t V_t + (C_m \parallel C_c) V_m}{C'_t} && \approx \frac{C_t V_t + C_c V_m}{C_t + C_c} \\ C'_c &= C_m + C_t + \frac{C_m C_t}{C_c} && \approx C_m \left(1 + \frac{C_t}{C_c}\right) \end{aligned}$$

The approximations are valid in the case of a big main dot and a much smaller trap ($C_m^i \gg C_t^j, C_c$), and we have defined $C_1 \parallel C_2 \equiv (C_1^{-1} + C_2^{-1})^{-1}$. $C_1 \parallel C_2$ therefore gives the series capacitance of C_1 and C_2 . The expressions for $C'_{m,t}$ and $V'_{m,t}$ can be understood easily from Fig. 1(c).

As we focus on the general structure of the Coulomb blockade spectrum and not on the exact conductance values we simplified the problem by considering equal and constant transmission coefficients of the main dot towards source and drain. For the coupling of the trap towards source and main dot, we supposed equal and very weak transmission coefficients. Electrons can therefore be added or removed from the trap, but their contribution to the total current through the device can be neglected. This contrasts with models of stochastic Coulomb blockade⁸ or in-series quantum dots^{9,10} where the current has to pass through both dots.

In terms of kinetic energy, we describe the main dot as metallic (negligible single-particle level spacing Δ , i.e. $\Delta \ll kT$) and for the trap we consider only one non-degenerate energy level. In source and drain we suppose a uniform density of states. The transition rates of an electron in the main dot to the source or drain reservoirs or from the reservoirs to the dot are then proportional to the auto-convolution of the Fermi function. The transition rates from or towards the trap are directly proportional to the Fermi function.¹¹

The statistical probability for each state $|N_m, N_t\rangle$ of the system ($N_{m,t}$ are the numbers of electrons in the main dot and the trap) can now be calculated by solving numerically the master equation. The probability for each state allows then to calculate the mean current through the system, which we compare to the measurements.

IV. INTERPRETATION

The result of a simulation is plotted in Fig. 4. The parameters have been chosen to reproduce the data in Fig. 3: we used $T = 1$ K for the effective temperature;

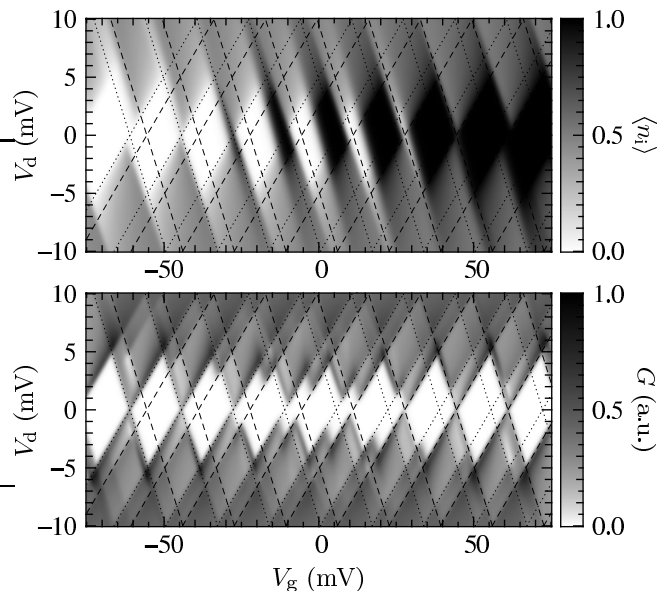


FIG. 4: Numerical study of a trap coupled to the source and to the main quantum dot, as sketched in Fig.1(b). The trap can either be empty or charged with one electron. The upper panel shows the self-consistent mean occupation number of the trap, the lower panel the resulting conductance through the dot. The parameters for this simulation have been chosen close to the experimental ones (see text). The effect of the charge trap is to shift the Coulomb blockade diamonds of the main dot depending on the charge in the trap. The dotted (dashed) lines indicate the position of the diamonds when the trap is empty (occupied). This result is in very good agreement with the experimental data shown in the lower panel of Fig. 3.

$C_m^g = 60 \frac{e}{V}$, $C_m^d = C_m^s = 70 \frac{e}{V}$ for the main dot; $C_t^g = 0.045 \frac{e}{V}$, $C_t^s = 2 \frac{e}{V}$, $C_t^d = 0$ for the trap and $C_c = 1 \frac{e}{V}$ for the coupling. The barrier transmissions between dot and source and between dot and drain are taken equal and constant, while the transmissions between trap and source and between trap and dot are taken 1000 times smaller.

This simulation only addresses statistical mean values of current and occupation probabilities. In reality, as the transmission rates are low, the trap will be occupied or empty for a fairly long time. This should be observable as random telegraph noise.^{2,3,12} Indeed we observed stronger noise near these anomalies. Although the presented low frequency measurements are not fast enough to observe directly this random telegraph noise, it is readily visible with a spectrum analyzer.

The top panel of Fig. 4 shows the mean occupation of the trap. Globally, the trap becomes occupied with increasing gate voltage. However every time a new electron is added onto the main dot the interaction term in Eq. (1) increases and it becomes once again favorable to empty (discharge) the trap. But due to the gate-voltage dependent term in Eq. (1), at each cycle the region where the trap is occupied becomes larger.

Inversely, when the trap becomes occupied, the interaction term shifts the Coulomb blockade structure of the main dot to higher gate voltage. The two Coulomb blockade structures for unoccupied and occupied trap are respectively indicated by dotted and dashed lines in Fig. 4.

The shift between these two cases is given by

$$\delta V_g = \frac{e}{\left(1 + \frac{C_t}{C_c}\right) C_m^g + C_t^g} \approx V_g^C \frac{1}{1 + \frac{C_t}{C_c}} \quad (2)$$

In the limit of a small trap ($C_t^g \ll C_m^g$) it does not depend on the absolute value of the coupling capacitance C_c but only on the ratio of the capacitive coupling towards the electrodes and towards the dot. The effect is the strongest ($\frac{\pi}{2}$ shift) when these two capacitances are equal. So even a trap far from the quantum dot can have a strong influence, as long as the coupling to the electrodes or ground is also weak. The entire trap signature is independent of the absolute value of the trap capacitances ($C_m^i \gg C_t^j, C_c$): An multiplication of C_t^i and C_c by a same factor does not modify the result in Fig. 4. Therefore we cannot determine the absolute value of the trap's coupling capacitances and charging energy. This would only be possible if at least two signatures could be attributed to one trap being occupied successively with two or more electrons.

The width in gate voltage ΔV_g of an anomalous zone at low drain voltage can be estimated as follows. The electrostatic potential W is the only significant contribution the the thermodynamical potential at low temperature and chemical potential $\mu = 0$ in source and drain, and therefore determines the ground state of the system. We consider the charge on the main dot Q_m at first as continuous and we can find charges $Q_m^{0/1}$ that minimize $W(Q_m^1, -e)$ and $W(Q_m^0, 0)$ respectively. The difference $\Delta W_{\min} = W(Q_m^1, -e) - W(Q_m^0, 0)$ indicates whether the trap is empty ($\Delta W_{\min} > 0$) or occupied ($\Delta W_{\min} < 0$) at low temperature. For a continuous charge Q_m the trap changes its state once when gate voltage is swept. The finite width of the zone where the two dots interact is introduced when we take into account the discrete nature of the charge Q_m : The deviation from the optimal charge is at most $\frac{e}{2}$. This leads to a maximum deviation from the minimum energy for continuous charge of $\delta W = \frac{e^2}{8C_m^g}$ (see Eq. (1)). At zero bias, ΔW_{\min} has to change from $-\delta W$ to $+\delta W$ in order to toggle the trap from always empty to always occupied. It has therefore to change by $\frac{e^2}{4C_m^g}$. This corresponds (in the limit $C_m \gg C_t$) to a change in gate voltage of

$$\Delta V_g = \frac{e}{4} \frac{C_t + C_c}{C_m C_t^g} \quad (3)$$

This equation can also be expressed as:

$$\begin{aligned} \frac{C_t^g}{C_t + C_c} &= \frac{1}{4n} \frac{C_m^g}{C_m} \\ \alpha_t &= \frac{1}{4n} \alpha_m \end{aligned} \quad (4)$$

where n is the number of anomalous periods. α_m is the gate-voltage lever-arm of the main dot when the charge in the trap is fixed, i.e. $\alpha_m = \frac{\partial V_m'}{\partial V_g} \approx \frac{C_m^g}{C_m}$. For the lever-arm α_t of the trap, however, we have to consider the charge of the main dot at equilibrium. As above we approximate it as continuous. Thus

$$\alpha_t = \frac{d\Delta W_{\min}}{-e dV_g} = \frac{C_t^g}{C_t'} \left(1 - \left(\frac{C_c}{C_m + C_c}\right)^2\right) \approx \frac{C_t^g}{C_t + C_c} \quad (5)$$

The bottom panels of Figs. 3 and 4 show five anomalous periods. With the lever arm for the main dot $\alpha_m = 0.3$, Eq. (4) gives thus $\alpha_t = 0.015$. With the parameters for the simulation in Eq. (5) we calculate the exact value $\alpha_t = 0.0148$. The excellent agreement validates Eq. (4).

With the informations obtained so far we can estimate the position of the trap. First, we locate the trap perpendicularly to the wire: The gate-voltage lever-arm being low, the trap cannot be near the gate electrode. Traps located deep inside the oxide can also be excluded because their transmissions would be too weak to observe statistical mixing of occupied and unoccupied trap states during our acquisition time of about 1 s. Similar devices including intentional silicon nanocrystals at the interface between thermal oxide and deposited oxide have been studied in views of memory applications.^{13,14} The measured lifetime of charges in the nanocrystals exceeds 1 s already at room temperature. The traps must therefore be inside the Si wire or at its interface with the oxide. The interface traps are unlikely: We estimate their density to be smaller than 10^{10} cm^{-2} , corresponding to a few units per sample. As they are distributed throughout the entire band gap it is very unlikely to observe several of them in the small energy window $\alpha_t (V_g^{\max} - V_g^{\min}) \approx 30 \text{ meV}$ that we scan in our measurement. The most likely candidates are therefore defects in the silicon wire or As donor states.⁶ Given the volume of the access regions under the spacers and the doping level N_D , there are around 70 donor states per device. We estimate the width of the impurity band to be $\frac{e^2}{\epsilon_0 \epsilon_r N_D^{-1/3}} \approx 150 \text{ meV}$.⁶ One should therefore expect to observe in the order of 15 impurities in the energy window. We record typically 3 to 5 impurities. The estimation is crude and the relatively small discrepancy is not surprising as we expect the Fermi-level not exactly at the center of the impurity band where the density of states is highest. In addition, according to Eq. (2), traps very close to the dot ($C_c \gg C_t$) or very close to source or drain ($C_t \gg C_c$) are difficult to detect.

We discuss now the position along the nano-wire. The general structure of the trap signature indicates on which side of the dot the trap is: If teeth of constant width for all anomalous resonances are visible at the positive slope of the Coulomb blockade diamonds (as in the bottom panels of Figs. 3 and 4), the trap is on the source side of the dot. If they are visible at the negative slope, the trap is on the drain side. The width of these teeth is given by the shift between the Coulomb blockade diamonds for

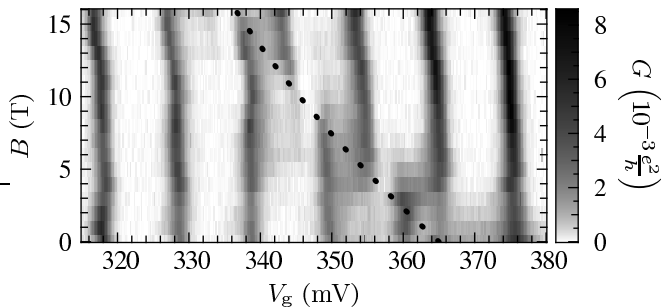


FIG. 5: Shift of a trap signature with magnetic field. The dotted line indicates the Zeeman shift expected for a trap state being occupied by a first electron it depends on the gate-voltage lever-arm which in turn is determined by the width of the signature. This prediction of the Zeeman shift follows exactly the observed shift.

empty and occupied trap (see lines in Fig. 4). In the case of Figs. 3 and 4 it is approximately $\frac{1}{3}$ of a Coulomb blockade period. According to Eq. (2) this gives a capacitance ratio $\frac{C_t}{C_c} = 2$. Knowing that $C_t \approx C_t^s$, we can translate this ratio into distance and find that the trap is located under the Si_3N_4 spacer, approximately 15 nm from the edge of the spacer on the source side, as sketched in Fig. 1(b).

Charge traps at very different positions could also be responsible for other effects. Traps whose coupling to the dot is much *stronger* than to ground could produce lines inside the conducting regions as in the top panel of Fig. 3 (The spacing between the lines is identical for all resonances and too high to be explained by excited states of the dot.)

A large number of traps whose coupling to the dot is much *weaker* than to ground could broaden the Coulomb blockade resonances¹⁵ and increase therefore the effective electronic temperature in our devices. Such traps can be found in the bulk silicon which is separated from the SOI wire by 400 nm of silica. It is weakly doped (B , 10^{15} cm^{-3}). At low temperature charges become therefore localized in the dopant states, but rearrangements of charges among these states could somewhat shift the Coulomb blockade structure. In time average one should observe broadened Coulomb blockade resonances. We expect a lower electronic temperature in further samples where a back-gate will shield the device.

V. SPIN

The spin of the trap state leads via the Zeeman energy under magnetic field to a gate-voltage shift of the trap signature of:

$$\frac{\partial V_g}{\partial B} = \alpha_t^{-1} g \mu_B \Delta S_z \quad (6)$$

μ_B is the Bohr magneton, ΔS_z the change in spin quantum number of the trap state in direction of the mag-

netic field when an electron is added to the trap. It can take the values $\pm \frac{1}{2}$. If there are already electrons in the trap higher changes are also possible, but they imply spin flips and such processes are therefore expected to be very slow.¹⁶ The Landé factor g for impurities in Si and SiO_2 has been measured by electron spin resonance.¹⁷ The observed renormalizations are beyond the precision of our measurements, therefore we take $g = 2$. The gate-voltage lever-arm of the trap states α_t is very weak as we have shown above. The Zeeman shifts should therefore be strong.

Indeed, the magnetic field clearly shifts the trap signature in Fig. 5 to lower gate voltage. In order to identify the shift as the Zeeman effect, we compare it quantitatively with the prediction of our model: The lever arm for the main dot is for this gate voltage $\alpha_m = \frac{C_m^g}{C_m} = 0.26$ and the width of the trap signature varies from 2.5 periods without magnetic field to 1.5 periods at 16 T. This implies a gate-voltage lever-arm for the trap of $\alpha_t = 0.026 \dots 0.043$ (see Eq. (4)). We interpolate it linearly in function of magnetic field. The dotted line in Fig. 5 is obtained if we put this lever-arm and $S_z = -\frac{1}{2}$ in Eq. (6). It is in very good agreement with the measured shift. The unrenormalized Landé factor is therefore justified a posteriori. The increase of the lever arm with magnetic field could be due to shrinking of localized states in the access regions: The nanowire is close to the metal-insulator transition where the dielectric constant diverges with the localization length.¹⁸ The increase of α_t under magnetic field could be due to shrinking of the localized states under magnetic field.⁶ This would reduce the dielectric constant and thus the coupling of the trap state towards source and dot, leading to an increase of the lever arm.

We observe such Zeeman shifts in the majority of our samples. In most cases the trap signature shifts to lower gate voltage as in Fig. 5. This is what we expect for traps occupied with one electron, because at low temperature the electron occupies the spin state whose energy is lowered by the Zeeman effect. When a trap state is occupied with a second electron it has to occupy the energetically less favorable state whose energy is increased by the Zeeman effect. This leads to a shift towards higher gate voltage under magnetic field. Although isolated As-donor sites in Si can only be occupied by one electron due to Coulomb repulsion, clusters of two donors could contain two or more electrons.¹⁹ For not too high doping levels clusters should however be rare. Accordingly we observe much less shifts to higher than to low gate voltage. This is in contrast with the reported shifts to higher energy for all traps in Refs. 2,3.

However, in some samples we found regularly spaced anomalies probably due to a larger impurity dot filled with several electrons. In these samples the current besides the anomalous regions is suppressed at low temperature, indicating that the impurity dot is in series with the main dot.^{8,10} In these cases we could not observe a clear Zeeman shift. Such anomalies are rather due to

larger structural defects, i.e. constrictions or dislocations that occupy the whole wire cross-section than to chemical impurities as the signatures described in this work. However, they could also be due to larger dopant clusters that can arise for randomly distributed dopants.¹⁹

VI. CONCLUSION

We interpreted anomalies in the Coulomb blockade spectrum of silicon quantum dots by charge traps in the low doped access regions. The experimental data are well

reproduced by simulations involving charge traps capacitively coupled to the main dot. They affect the Coulomb blockade characteristics of the main dot even for very weak coupling (both in terms of capacitance and transmission). A detailed analysis of the resulting signatures in function of applied voltages and magnetic field allowed us to determine the position and spin of the traps. Considering their occurrence we identified them as As donor states.

This work was partly supported by the European Commission under the frame of the Network of Excellence ‘‘SINANO’’ (Silicon-based Nanodevices, IST-506844)

-
- * Electronic address: max.hofheinz@cea.fr
- ¹ L. Besombes, Y. Léger, L. Maingault, D. Ferrand, H. Mariette, and J. Cibert, *Phys. Rev. Lett.* **93**, 207403 (2004).
 - ² M. Xiao, I. Martin, and H. W. Jiang, *Phys. Rev. Lett.* **91**, 78301 (2003).
 - ³ M. Xiao, L. Martin, E. Yablonovitch, and H. W. Jiang, *Nature* **430**, 435 (2004).
 - ⁴ J. M. Elzerman, R. Hanson, L. H. W. van Beveren, B. Witkamp, L. M. K. Vandersypen, and L. P. Kouwenhoven, *Nature* **430**, 431 (2004).
 - ⁵ D. E. Grupp, T. Zhang, G. J. Dolan, and N. S. Wingreen, *Phys. Rev. Lett.* **87**, 186805 (2001).
 - ⁶ B. I. Shklovskii and A. L. Efros, *Electronic properties of doped semiconductors*, no. 45 in *Solid State Sciences* (Springer, 1984).
 - ⁷ M. Boehm, M. Hofheinz, X. Jehl, M. Sanquer, M. Vinet, B. Prevtali, D. Fraboulet, D. Mariolle, and S. Deleonibus, *Phys. Rev. B* **71**, 33305 (2005).
 - ⁸ I. M. Ruzin, V. Chandrasekhar, E. I. Levin, and L. I. Glazman, *Phys. Rev. B* **45**, 13469 (1992).
 - ⁹ F. R. Waugh, M. J. Berry, D. J. Mar, R. M. Westervelt, K. L. Campman, and A. C. Gossard, *Phys. Rev. Lett.* **75**, 705 (1995).
 - ¹⁰ L. P. Rokhinson, L. J. Guo, S. Y. Chou, D. C. Tsui, E. Eisenberg, R. Berkovits, and B. L. Altshuler, *Phys. Rev. Lett.* **88**, 186801 (2002).
 - ¹¹ See for example H. Grabert and M. H. Devoret, eds., *Single charge tunneling: Coulomb blockade phenomena in nanostructures*, vol. 294 of *NATO ASI series, series B: Physics* (Plenum Press, 1992).
 - ¹² T. M. Buehler, D. J. Reilly, R. P. Starrett, V. C. Chan, A. R. Hamilton, A. S. Dzurak, and R. G. Clark, *J. Appl. Phys.* **96**, 6827 (2004).
 - ¹³ G. Molas, B. D. Salvo, G. Ghibaudo, D. Mariolle, A. Toffoli, N. Buffet, R. Puglisi, S. Lombardo, and S. Deleonibus, *IEEE Trans. Nanotech.* **3**, 42 (2004).
 - ¹⁴ G. Molas, X. Jehl, M. Sanquer, B. D. Salvo, D. Lafond, and S. Deleonibus, to appear in *IEEE Trans. Nanotech.*
 - ¹⁵ The effect of a large Coulomb island on a single electron transistor has been studied theoretically in R. Berkovits, F. von Oppen, and Y. Gefen, *Phys. Rev. Lett.* **94**, 76802 (2005).
 - ¹⁶ D. Weinmann, W. Häusler, and B. Kramer, *Phys. Rev. Lett.* **74**, 984 (1995).
 - ¹⁷ P. M. Lenahan and J. F. Conley, *J. Vac. Sci. Technol., B* **16**, 2134 (1998).
 - ¹⁸ T. G. Castner, N. K. Lee, G. S. Cieloszyk, and G. L. Salinger, *Phys. Rev. Lett.* **34**, 1627 (1975).
 - ¹⁹ R. N. Bhatt and T. M. Rice, *Phys. Rev. B* **23**, 1920 (1981).